Azadeh Jafari, Farzin Ghanadi, Matthew J. Emes, Maziar Arjomandi, Benjamin S. Cazzolato
Measurement of unsteady wind loads in a wind tunnel: Scaling of turbulence spectra
Journal of Wind Engineering and Industrial Aerodynamics, 2019; 193:103955-1-103955-11

Measurement of unsteady wind loads in a wind tunnel: scaling of turbulence spectra

Azadeh Jafari*, Farzin Ghanadi, Matthew J. Emes, Maziar Arjomandi, Benjamin S. Cazzolato
School of Mechanical Engineering, University of Adelaide, Adelaide, Australia

Abstract

Mismatch of turbulence spectra from the corresponding full-scale conditions is a common challenge in wind tunnel modelling of unsteady wind loads on small-scale structures, such as solar panels, heliostats and low-rise buildings. Understanding the effect of this mismatch on the unsteady wind loads is necessary for providing an accurate estimation of wind loads on full-scale structures. The correlation between the turbulence spectra and the unsteady wind loads in wind tunnel measurements is investigated in this study through measurement of unsteady lift and drag forces on horizontal and vertical flat plates. It was found through spectral analysis that the turbulent eddies in the range of reduced frequencies between 0.01 and 1 contributed the most to the unsteady wind loads. An approach for wind tunnel modelling was proposed in which the geometric scaling ratio of each model is determined based on the analysis of the turbulence power spectrum as a function of reduced frequency. The suitable geometric scaling ratio should be then chosen such that the turbulence spectrum as a function of reduced frequency is the closest match to that at full-scale for reduced frequencies between approximately 0.01 and 1.

Keywords: Unsteady wind load, turbulence spectrum, wind tunnel modelling, atmospheric boundary layer.

Nomenclature

A_D	aerodynamic admittance of the drag force
A_L	aerodynamic admittance of the lift force
c	characteristic length dimension (m)
C_D	drag coefficient
C_L	lift coefficient
$C_{L,0}$	lift coefficient at zero angle of attack
C_L'	slope of the lift curve near zero angle of attack (rad^{-1})
F	lift force (N)
f	frequency (Hz)

I_u	longitudinal turbulence intensity (%)
I_w	vertical turbulence intensity (%)
L_u^x	longitudinal integral length scale (m)
L_w^x	vertical integral length scale (m)
R	autocorrelation of velocity
S_{C_D}	power spectral density of the drag force coefficient (s)
S_{C_L}	power spectral density of the lift force coefficient (s)
S_{uu}	power spectral density of the longitudinal velocity fluctuation (m^2/s)
S_{ww}	power spectral density of the vertical velocity fluctuation (m^2/s)
t	time (s)
τ_u^x	longitudinal integral time scale (s)
u'	fluctuating velocity component (m/s)
U	mean velocity (m/s)
u, v, w	velocity components in the stream-wise, lateral and vertical directions (m/s)
x, y, z	distance in the stream-wise, lateral and vertical directions (m)
z_0	aerodynamic surface roughness (m)
z_{WT}	height in the wind tunnel (m)
z_{FS}	height in full scale (m)
Symbols	
α	angle of attack (°)
σ_u	standard deviation of longitudinal velocity fluctuations (m/s)
ρ	density (kg/m^3)

1 Introduction

Accurate estimation of the unsteady wind loads on structures is necessary for assessment of structural survivability under extreme conditions and prediction of the dynamic response. Several studies in the literature have used boundary layer wind tunnel testing for investigation of the wind loads on large civil structures such as buildings, bridges, as well as small-scale structures such as solar panels. While the common practice in wind tunnel testing is to generate a boundary layer with a logarithmic mean velocity profile similar to that of the atmospheric surface layer (ASL), similarity of the turbulence characteristics of the flow is also important for an accurate prediction of the unsteady wind loads (Holmes, 2007). For wind tunnel experiments of large civil structures such as tall buildings and bridges, achieving similarity of the turbulence spectra, length scales and intensity is possible. However, for small-scale structures such as low-rise buildings, solar panels, billboards and heliostats, similarity of the turbulence characteristics is often compromised by the technical challenges. These challenges arise due to the much smaller dimensions of the structure compared to the atmospheric surface layer height. Boundary layer wind tunnels are typically built for testing large-scale buildings

and structures, and allow generation of a boundary layer with a depth of 1–3 m. The essential depth of the neutral ASL for wind engineering applications is between 275 m and 550 m (Davenport, 1960), which is the gradient height where the wind speed reaches a maximum and is dependent on the wind speed and terrain roughness. Therefore, the boundary layer is typically scaled by a factor in the order of 1:100 and 1:500 in wind tunnels. It is not technically feasible to model the small-scale structures with such scaling ratios due to the challenges in modelling the structural details and difficulty of measurement of the pressure and forces on the model. Furthermore, the interference effects of the measurement devices are a problem for such models. Therefore, these structures are, in practice, modelled at larger scaling ratios between 1:10 to 1:50. As a result of the larger model scales, the Reynolds number and the turbulence spectra in the experiments differ from the full-scale condition. While it has been shown that the Reynolds number equality in wind tunnel experiments can be circumvented for sharp-edged models as long as the Reynolds number is above 50,000 (Tieleman, 2003), the turbulence characteristics of the flow affect the wind loads, especially the fluctuating component, significantly.

The mismatch of the turbulence spectra due to the violation of the geometric scaling has led to a large variability in the reported wind load measurements from different wind tunnel experiments. For instance, a comparison of the maximum pressure coefficients on a cubic building model reported from six wind tunnel studies (Hölscher and Niemann, 1998), as displayed in Figure 1(a), shows a deviation of up to 12% between the peak pressure coefficients. All the six studies used a similar method for simulation of a neutral suburban boundary layer with an average power law exponent α=0.22, and the wind loads were measured at similar turbulence intensity (I_u =12%). However, the geometric scaling factors were different and the model height varied between 100 mm and 250 mm among the six studies. A similar comparative study was conducted to measure the pressure distribution on low-rise building models in an open-country (z_0=0.03 m) and a suburban terrain (z_0=0.3 m) in six wind tunnels (Fritz *et al.*, 2008). The peak pressure coefficient reported from the six studies varied between 1.2 and 3 for the open-country terrain and between 1.5 and 2.1 for the suburban terrain. This large variability was attributed to the difference in the ratio of the turbulence length scales and the model dimensions, as well as the measurement techniques (Fritz *et al.*, 2008). Furthermore, Stathopoulos and Surry (1983) found that changing the scaling ratio of a building model from 1:500 to 1:100 led to a reduction of the peak local pressure coefficient on the walls of the model by 30% for the same flow conditions. Another example of the discrepancies is the

wind load coefficients on heliostats reported by two wind tunnel experiments (Peterka *et al.*, 1989; Pfahl *et al.*, 2011) with a similar mean velocity profile and a similar turbulence intensity (I_u =18%). The main difference between the two studies was the geometric scaling ratio of the model, 1:40 and 1:20 for Peterka *et al.* (1989) and Pfahl *et al.* (2011), respectively. As shown in Figure 1(b), for instance the measured peak drag coefficient from the two studies differ by 30%. Furthermore, Emes *et al.* (2017) found that the peak lift coefficient on a heliostat at zero elevation angle increased from 0.3 to 0.83 as the model characteristic length decreased from 0.8 m to 0.3 m at a constant turbulence intensity (I_u =12.5%). The increase in the peak lift coefficient was attributed to the increase of the ratio of turbulent integral length scale to the model dimension (Emes *et al.*, 2017). Moreover, as demonstrated in Figure 1(c), a comparison between the measured peak pressure coefficients on a rooftop solar panel in a wind tunnel study (at scaling factor of 1:24) and a full-scale measurement shows that the peak pressure coefficients are underestimated in the wind tunnel experiment (Stathopoulos *et al.*, 2012). Therefore, the geometric scaling ratio of the wind tunnel models is the main reason of the discrepancies in wind tunnel studies with similar mean flow conditions. Since wind tunnel experimentation is the primary tool for prediction of unsteady wind loads and due to the importance of an accurate estimation of the loads for the design of the structures, it is necessary to develop a standard method for accurate estimation of unsteady wind loads on small-scale structures.

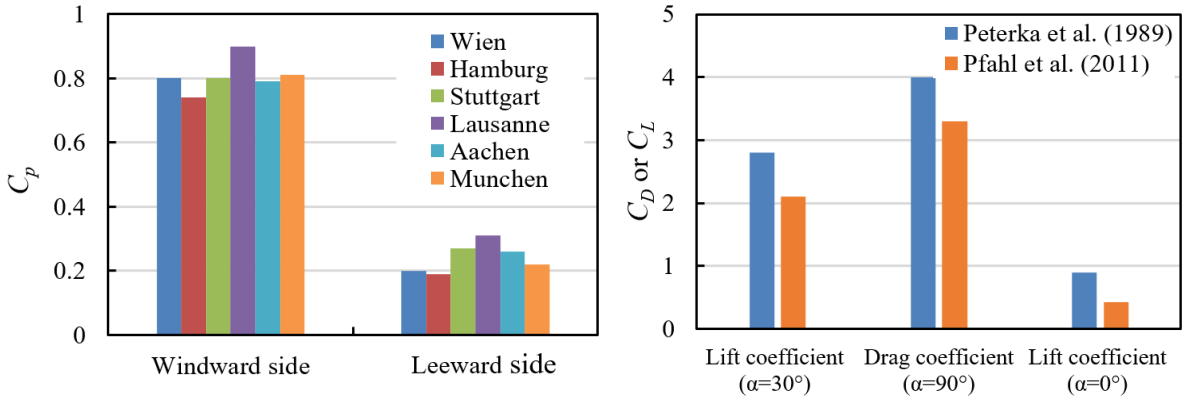

(a) (b)

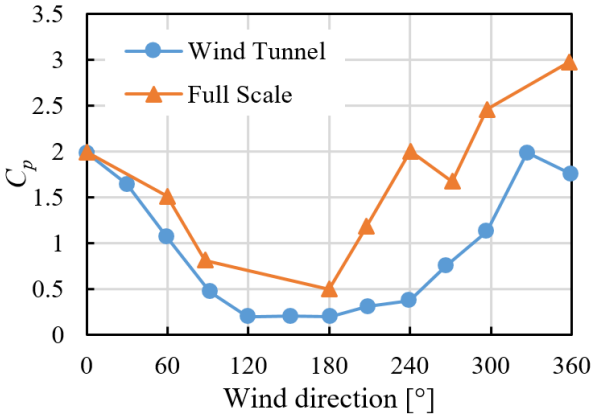

(c)

Figure 1: (a) Comparison of absolute maximum pressure coefficients, $C_p = P/0.5\rho U^2$, for a cubic building model from different wind tunnel studies, conducted at wind tunnels at six cities, with a similar mean velocity profile and an average turbulence intensity of 12% reproduced from Hölscher and Niemann (1998), (b) comparison of peak lift and drag coefficient at different elevation angles of heliostats from two wind tunnel studies (Peterka *et al.*, 1989; Pfahl *et al.*, 2011), (c) comparison of absolute maximum pressure coefficients, $C_p = P/0.5\rho U^2$, for a solar panel on a 30-degree hipped roof reproduced from Stathopoulos *et al.* (2012).

Reduction of turbulence intensity in wind tunnel tests has been proposed as a method to alleviate the mismatch of turbulence spectra (Dyrbye and Hansen, 1996). The common practice of matching turbulence intensity in the wind tunnel experiments to that at full-scale leads to a shift of the power spectra to higher frequencies. Dyrbye and Hansen (1996) recommended that by reducing turbulence intensity in the wind tunnel experiments, the high frequency range of the spectrum can be matched to that of the full-scale. However, similarity of the whole spectrum cannot be achieved. Hence, the remaining argument is whether the whole turbulence spectrum needs to be matched or similarity of a specific frequency range is sufficient for measurement of the wind loads in the wind tunnel experiments. In other words, the frequency range of the turbulence power spectrum which is more effective in generating the unsteady wind loads needs to be determined.

The peak of the turbulence spectrum containing the most energetic eddies, which is represented by the integral length scale of turbulence, is nominated as an important parameter which contributes significantly to the wind loads in the literature. For instance, the drag coefficient on a flat plate normal to a turbulent flow with a longitudinal turbulence intensity I_u=8% is found to be strongly dependent on the ratio of the longitudinal integral length scale to the characteristic length of the plate, L_u^x/c, such that the root-mean-square (RMS) of the drag coefficient increases dramatically by increasing L_u^x/c (Bearman, 1971). A similar trend is found for a flat plate normal to a simulated atmospheric boundary layer showing that the RMS of the drag coefficient increases by 37% when L_u^x/c increases from 1.5 to 4 at I_u=26%, and by 70% when L_u^x/c increases from 0.97 to 2.3 at I_u=13% (Jafari *et al.*, 2018). The mean drag force

on a rectangular prism is also found to be dependent on L_u^x/c (Lee, 1975). Furthermore, L_u^x/c is reported to be the factor responsible for the differences in the measured pressure distribution on cubic models of different scaling ratios (Holdø *et al.*, 1982). The area-averaged pressure coefficients on the leeward and windward faces of cubic building models of different scaling ratios in a boundary layer wind tunnel experiment are found to increase by 50% when L_u^x/c increased from 1 to 4 (Hunt, 1982). Roy and Holmes (1988) on the other hand correlated the fluctuating wind loads on models of low-rise buildings with the lateral integral length scale, L_u^y. The vertical integral length scale is also found to dominate the wind loads on a horizontal thin flat plate showing that the fluctuating wind loads increase with increasing L_w^x/c (Jafari *et al.*, 2019).

On the other hand, Tieleman (2003) argues that the integral length scale is not of primary influence on the peak pressure coefficient on low-rise buildings, but the high-frequency range of the spectrum needs to be matched in the wind tunnel modelling. The high frequency turbulence affects the flow separation and reattachment but the effect of the low frequency turbulence, which is of much larger length scale than the structure, is similar to the effect of changing the mean velocity vector (Tieleman, 2003). Furthermore, the pressure coefficients on a cube model in a wind tunnel boundary layer, in which the high frequency range of the turbulence spectrum was a close match to the full-scale, were found to be close to the full-scale pressure measurements on the Silsoe cube (Richards *et al.*, 2007). It was proposed that turbulence over the range of the non-dimensional frequencies fz/U>0.05 directly interacts with the local flow field and is therefore important to be modelled accurately in the wind tunnel. The results of this study show that the scale of turbulence in relation to the mean velocity and the structure dimensions are important. Furthermore, Aly and Bitsuamlak (2013) measured the pressure coefficient on ground-mounted solar panels of different scaling ratios and recommended that by matching the turbulence spectra at high frequencies and calculating the average of peak pressure coefficients for measurement periods of 3 seconds, the 3-second pressure coefficients for the models with different scaling ratios will be similar. A quantitative analysis of the effect of the lower frequencies on the peak pressure is however not given.

A review of the existing literature shows that the correlation between the turbulence power spectrum of the flow and the fluctuating wind loads is not known. While some of the studies in the literature (Lee, 1975; Holdø *et al.*, 1982; Hunt, 1982; Roy and Holmes, 1988) indicate the peak of the turbulence power spectra to be more important for the unsteady wind loads, other studies (Tieleman, 2003; Richards *et al.*, 2007) propose that the high frequency range to

be dominant. Determination of the critical frequency range of the spectrum which contributes to the generation of the unsteady wind loads is required for wind tunnel modelling of the small-scale structures. Hence, the aim of this study is to develop an understanding of the correlation between the turbulence spectra and the unsteady wind loads by spectral analysis of the turbulence of wind tunnel boundary layers and the fluctuating forces on flat plate models of various geometric scaling ratios. The flat plate is studied as a fundamental geometry to establish a standard method. The implemented method is described in Section 2, followed by analysis of the turbulence characteristics of the simulated atmospheric boundary layers in the wind tunnel in Section 3. Their resemblance to the atmospheric turbulence and the existing mismatch of the spectra for modelling the small-scale structures are then described. In Section 4, the experimental measurements of the forces on horizontal and vertical flat plates in the wind tunnel boundary layers are presented, and the correlation between the turbulence spectra and the unsteady forces on the plates is investigated by determination of the aerodynamic admittance function. A case study is then discussed in Section 5 to demonstrate how the results of this study can be applied for wind tunnel modelling of a flat-plate-like structure. The results of this study can be applied for a more accurate wind tunnel modelling of small-scale structures such as solar panels, heliostats and billboards.

2 Methodology

Wind loads on thin square flat plates of different characteristic lengths, resembling different geometric scaling ratios, in vertical and horizontal configurations were measured in simulated boundary layers in the large-scale wind tunnel at the University of Adelaide. The rectangular test section of the boundary layer wind tunnel has a cross-sectional area of 3 m × 3 m, and the level of turbulence intensity in the empty tunnel is between 1% and 3% outside the boundary layer. Two wind tunnel boundary layers (WTBL) with different intensities and length scales of turbulence were generated using two sets of spires and roughness elements. For each WTBL, three spires with identical dimensions, shown in Figure 2(a), were placed at a centre-line distance of 0.9 m in the lateral (y) direction followed by a 10 m stream-wise fetch of wooden roughness elements (90 mm × 90 mm cross section and 45 mm height). The sizing and spacing of the roughness elements were determined using the empirical equations by (Wooding *et al.*, 1973). The elements were placed with a spacing of 500 mm in all directions covering approximately 24% of the floor area over the fetch length. The spires were designed based on Kozmar's part-depth method (Kozmar, 2011) for part-depth simulation of the atmospheric

boundary layer. The flat plates were placed downstream of the spires at a distance equal to 6 times the spire height which is expected to be sufficient for flow development (Irwin, 1981). Square flat plates with chord length dimensions between 0.2 m and 0.7 m with a thickness of 3 mm were mounted on a post of constant height (0.3 m). The forces on the horizontal and vertical flat plates were measured by three three-axis ME load cells (K3D50), each with a capacity of 50 N which were calibrated for a range of forces between 0-25 N. A schematic of the wind engineering test section of the tunnel containing spires and roughness elements and the flat plate model is shown in Figure 2(b).

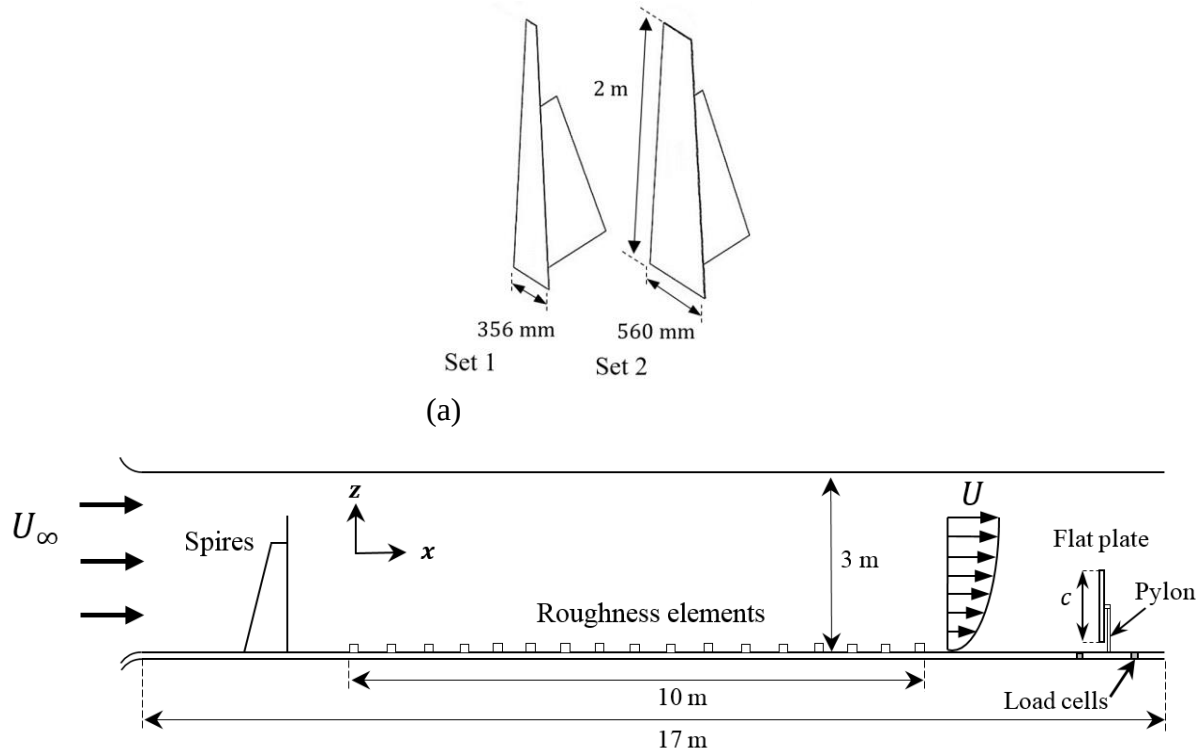

Figure 2: (a) Dimensions of the two spire sets, (b) Schematic of the test section containing spires and roughness elements and the flat plate model.

2.1 Calculation of turbulence characteristics within the WTBL

Three components of velocity (u, v, w) were measured by a Turbulent Flow Instrumentation (TFI) multi-hole pressure probe, with an accuracy of ±0.5 m/s, downstream of the roughness fetch over an area of 1 m^2 in both vertical and lateral directions, with a longitudinal spacing of 500 mm in order to investigate flow development. Data were measured for a duration of 150 s at each location at a sampling rate of 1 kHz. In order to reduce the experimental errors, the velocity measurements were repeated for five times and the average of the five measurements was calculated. Turbulence intensity was calculated from the following:

$$I_i = \frac{\sigma_i}{U}, i = u, w \quad (1)$$

The power spectral densities of the velocity fluctuations were found using the *pwelch*-function in MATLAB.

2.2 Calculation of wind load coefficients

The forces on the flat plates were sampled at 1 kHz and were measured over a sampling period of 120 seconds, which was found to be sufficient as the calculated root mean square (RMS) of the fluctuating forces varied by less than 2% when the sampling period increased above 120 seconds. Only the dominant unsteady wind-induced force, which is the force acting normal to the plate, the drag force for the vertical flat plate and the lift force for the thin horizontal flat plate, were reported for all cases. Since the turbulence characteristics of the flow mainly impact the unsteady wind loads, only the unsteady wind load coefficients are reported in this study.

The fluctuating drag and lift coefficients were calculated from the following:

$$C_{i,RMS} = \frac{F_{i,RMS}}{\frac{1}{2}\rho U^2 c^2}, \quad i = L, D \quad (2)$$

where $F_{i,RMS}$ represents the RMS of the fluctuating component of lift and drag forces, ρ represents the air density, U is the mean velocity at pylon height and c represents the characteristic length of the flat plate.

3 Characterisation of the WTBLs

The mean velocity profile at the centre-line (y=0) as a function of height in the wind tunnel boundary layers generated by the two sets of spires and roughness elements, hereafter referred to as WTBL1 and WTBL2, at a freestream velocity of 11.5 m/s is shown in Figure 3, which match the logarithmic profiles corresponding to the atmospheric surface layer. The aerodynamic surface roughness lengths were determined by fitting the mean velocity profile of each simulation to the logarithmic law. As shown in Figure 3, the velocity profile of WTBL1 matches a logarithmic profile with a roughness height of 0.018 m in full scale, with a maximum error of 2.3%, and represents an open country terrain. The mean velocity profile of WTBL2 matches a logarithmic profile with a roughness height of 0.35 m and a displacement height of 0.02 m in full scale, with a maximum error of 5% (for heights up to 0.7 m), and is representative of a suburban terrain. It must be noted that the displacement height is negligible for terrains whose surface roughness value is low (such as flat and open country terrains), while for

suburban and urban terrains, the displacement height is non-zero (Holmes, 2007; Kozmar, 2012; De Paepe *et al.*, 2016). Therefore, the displacement height (equal to 0.02 m in full scale) is found for the logarithmic profile fit of the mean velocity profile of WTBL2 with z_0=0.35 m. The longitudinal and vertical turbulence intensities within WTBL1 and WTBL2 are shown in Figure 4. Longitudinal turbulence intensity within the WTBLs decrease with height. According to Figure 4, the longitudinal turbulence intensity reduces from 15% to 9% in WTBL1 and from 34% to 20% in WTBL2 as the height from the ground increases to 1 m. The variation of turbulence intensity with height from the ground is larger in WTBL2 since the aerodynamic surface roughness is larger, whereas for WTBL1, which resembles an open-country terrain with lower surface roughness, the change in turbulence intensity with height is less. At the model height at 0.5m, the longitudinal turbulence intensity is approximately 11% and 26%, and the vertical turbulence intensity is approximately 9% and 21% within WTBL1 and WTBL2, respectively.

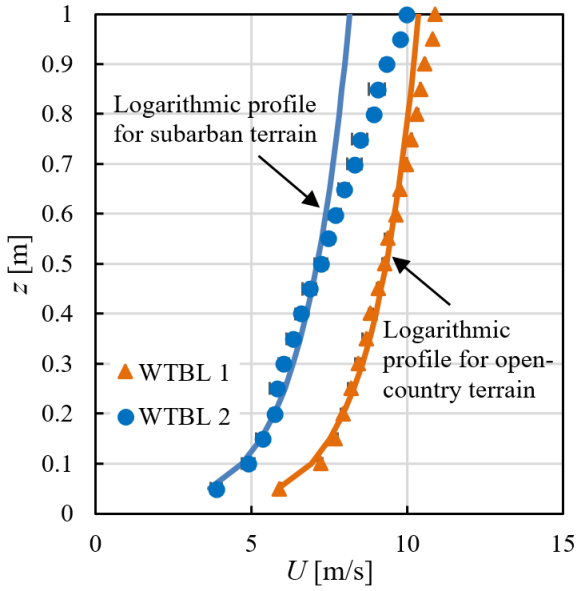

Figure 3: Mean velocity profile of the wind tunnel boundary layers compared with logarithmic profiles. The error bars show the standard deviation calculated from five measurements.

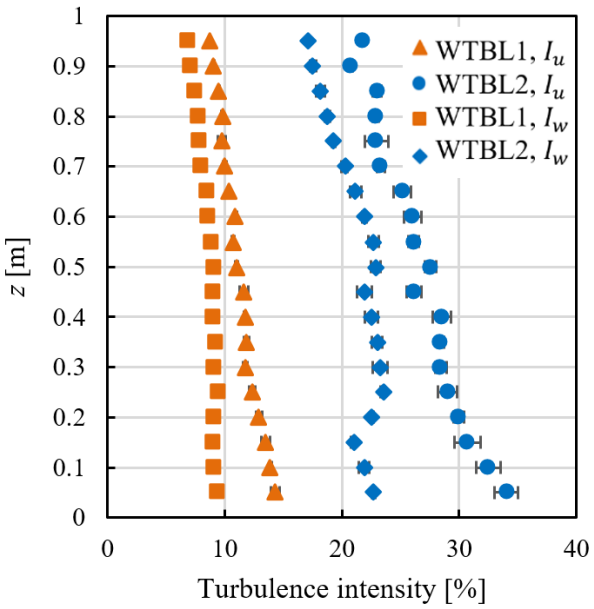

Figure 4: Longitudinal turbulence intensity profiles for WTBL1 and WTBL2. The error bars show the standard deviation calculated from five measurements.

The longitudinal and vertical velocity spectra at different heights of 0.1 m, 0.3 m in WTBL1 and WTBL2 are shown in Figure 5, which shows that turbulence tends to be locally isotropic for fz/U above 0.3 in both boundary layers. The spectral distribution of vertical turbulence energy follows the same trends as those in the atmosphere having the +1 and -2/3 slopes. Three distinctive spectral ranges can be seen in the longitudinal power spectra in the wind tunnel boundary layers at the lower height, z= 0.1 m: The inertial subrange where $fS_{uu} \propto f^{-2/3}$; the lower frequency range, where S_{uu} is independent of f (the +1 slope for fS_{uu}/U^2); and a self-similar range, where fS_{uu}/U^2 is constant which extends over fz/U of about 0.02 to 0.06 (Högström *et al.*, 2002; Drobinski *et al.*, 2004). By increasing the height from the ground to z=0.3 m, the self-similar region almost disappears. The self-similar range has also been identified in the lower 10–20 m of the ASL, known as the eddy surface layer, from the measured atmospheric data from different sites (Högström *et al.*, 2002; Drobinski *et al.*, 2004). The self-similar range of the eddy surface layer represents the anisotropic eddies formed due to the blockage by the ground (Högström *et al.*, 2002). Therefore, the distribution of the turbulence energy in the wind tunnel boundary layers is similar to the lower part of ASL. It must be noted that the power spectral density is normalised by mean velocity and measurement height as recommended by Richards *et al.* (2007). This method of normalising the spectral density demonstrates the differences between the simulated boundary layers more clearly compared to normalising with turbulence dependant variables such as variance and integral length scale (Richards *et al.*, 2007).

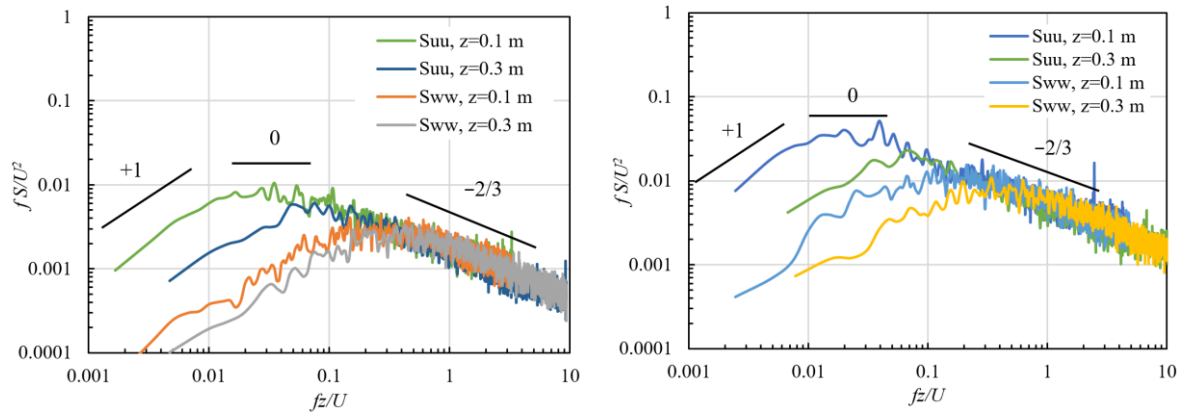

(a) (b)

Figure 5: Normalised longitudinal velocity spectrum, fS_{uu}/U^2, and normalised vertical velocity spectrum, fS_{ww}/U^2, as a function of fz/U, at different heights in (a) WTBL1 and (b) WTBL2.

3.1 Mismatch of turbulence spectra in modelling small-scale structures

The mismatch of turbulence spectra usually occurs when a small-scale structure is modelled in the wind tunnel as a result of the larger geometric scaling ratio of the model compared to that of the simulated boundary layer. The difference in the geometric scaling ratio of the structure and the boundary layer leads to a difference in the scale of flow turbulence in relation to the structure's characteristic length. The consequences of such violation of the similarity of geometric scaling ratio are further elaborated by an example. The simulation length scale factor for the wind tunnel boundary layers is calculated using Cook's method (Cook, 1978) from the aerodynamic surface roughness length and integral length scales at different heights within each boundary layer. The length scale factor for WTBL1 and WTBL2 was determined as the average of the calculated values from Cook's method for different heights. Hence, the simulation length scale factor was found to equal 1:151 and 1:90 for WTBL1 and WTBL2, respectively. A flat-plate-like structure with a characteristic length of 12 m at a height of z_{FS}=6 m in the full-scale is considered as an example. This flat plate could resemble an industrial heliostat or solar tracker. An accurate model of this flat plate in WTBL1 is required to be scaled down by a factor of 1:151, i.e., identical to the scaling ratio of the simulated boundary layer. The model is thus required to be composed of a plate of approximately 0.08 m by 0.08 m placed at a height of approximately 0.04 m in the wind tunnel. There are however several technical challenges for such small-scale wind tunnel testings such as interference effects of the measurement devices and requirement of very sensitive low-range force sensors. Therefore, the model is usually built at a larger scaling ratio, typically about 1:10 to 1:50, as done in the literature such as (Radu *et al.*, 1986; Peterka *et al.*, 1989; Bronkhorst *et al.*, 2010; Pfahl *et al.*, 2011; Ruscheweyh and Windhövel, 2011; Saha *et al.*, 2011; Emes *et al.*, 2017).

Taking a model scaling ratio of 1:20, the model will be composed of a plate of 0.6 m by 0.6 m placed at a height of 0.3 m. Figure 6 shows the longitudinal and vertical turbulence intensity profiles of WTBL1 converted to full-scale (by a factor of 1:151) along with the estimations of the atmospheric turbulence intensities given by ESDU85020 (2010) for a terrain with a similar surface roughness. The solid lines showing the ESDU range are represented as ±20% from the calculated mean values which is suggested as the allowable bandwidth (ESDU85020, 2010). The two horizontal lines show the full-scale height of the structure within the ASL (z_{FS}=6 m) and the corresponding full-scale height of the model in the wind tunnel (z_{WT}=0.3 m) which equals 45.3 m. As shown in Figure 6, with the model being placed at a larger height within the boundary layer (45.3 m opposed to z_{FS}=6 m), turbulence intensity at the model height is less than those given by ESDU85020 (2010) for z_{FS}=6 m.

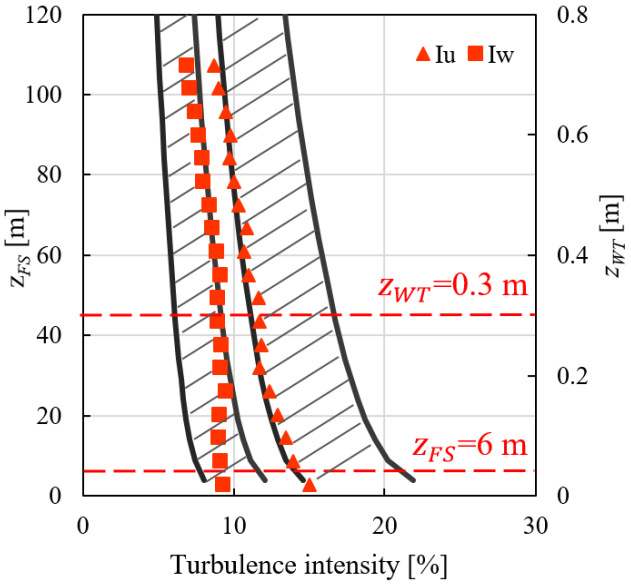

Figure 6: Longitudinal and vertical turbulence intensity profiles for WTBL 1 at the wind tunnel scale and at full-scale (scaling ratio 1:151). The shaded areas show the estimations by ESDU 85020 for z_0=0.018 m.

Furthermore, the spectral distribution of turbulence at the model position is very different from that at full-scale. This is shown by comparison of the normalised spectra at z_{WT}=0.3 m in WTBL1 with the full-scale spectra at z_{FS}=6 m and 45.3 m in Figure 7(a–b). The ASL spectra are estimated from the spectral equations given by ESDU85020 (2010) which provide a modified version of Von Karman's model. The ESDU spectral equations correct for the underestimation of the integral length scales and the overestimation of the peak of the spectra by the Von Karman model at lower heights near the ground (ESDU85020, 2010), and are therefore applied in this study to predict the turbulence spectra. According to Figure 7(a), the longitudinal turbulence spectrum at z_{WT}=0.3 m in WTBL1 almost matches that at 45.3 m in

full-scale. However, it deviates from the spectrum at z_{FS}=6 m over the mid and low frequencies. The peak of the longitudinal power spectrum at z_{WT}=0.3 m occurs at higher frequencies compared to the spectrum at z_{FS}=6 m, which indicates the integral length scale is smaller. Although, the higher frequency range, fz/U>0.1, at z_{WT}=0.3 m matches that at z_{FS}=6 m, the large-scale eddies in the wind tunnel contain lower turbulence energy than the full-scale z_{FS}=6 m. Furthermore, according to Figure 7(b), there is a distinctive shift to higher frequencies in the vertical power spectrum of WTBL1 at z_{WT}=0.3 m compared to the full-scale vertical spectrum at z_{FS}=6 m. Furthermore, according to Figure 7(b), there is a distinctive shift to higher frequencies in the vertical power spectrum of WTBL1 at z_{WT}=0.3 m compared to the full-scale vertical spectrum at z_{FS}=6 m. The peak of the vertical power spectrum at z_{WT}=0.3 m, occurs at fz/U=0.4 compared to the peak of the spectrum at z_{FS}=6 m at fz/U=0.02. Therefore, as shown in Figure 7(b), the vertical turbulence energy in the wind tunnel is composed of eddies of higher frequencies and relatively smaller length scales compared to the corresponding full-scale height.

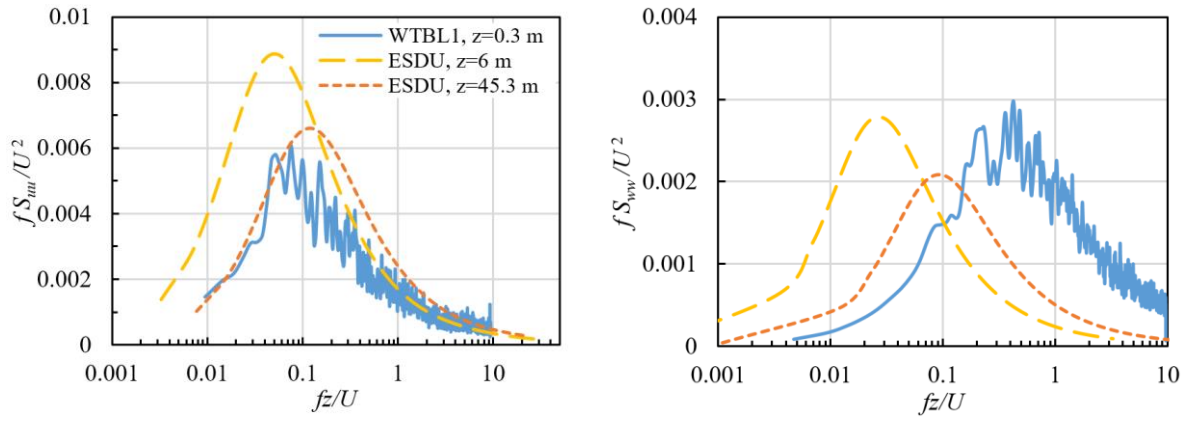

(a) (b)

Figure 7: Comparison of normalised spectral densities as a function of fz/U at z=0.3 m in WTBL1 with the ESDU estimations for the ASL spectra at a terrain with similar terrain roughness at two heights, (a) normalised longitudinal velocity spectrum, fS_{uu}/U^2, (b) normalised vertical velocity spectrum, fS_{ww}/U^2.

4 Experimental results

The unsteady wind loads on horizontal (α=0°) and vertical (α=90°) square flat plates of different characteristic length dimensions between 0.2 m and 0.7 m, resembling different geometric scaling ratios, were measured within WTBL1 and WTBL2. Figures 8 shows the RMS of the unsteady lift coefficient on the horizontal plates and the unsteady drag coefficient on vertical plates, respectively. Both the unsteady lift and drag force coefficients are found to decrease with increasing the characteristic length of the plate, which shows that the measured

wind forces in wind tunnel experiments vary significantly when the size of the model and its geometric scaling ratio change. For example, according to Figure 8(a), in WTBL2, increasing the characteristic length dimension of the plate from 0.2 m to 0.7 m reduces the fluctuating lift coefficient from 0.6 to 0.19. Similarly, Increasing c from 0.2 m to 0.7 m leads to a reduction in the fluctuating drag coefficient from approximately 0.39 to 0.22 and from 0.8 to 0.53 within WTBL1 and WTBL2, respectively.

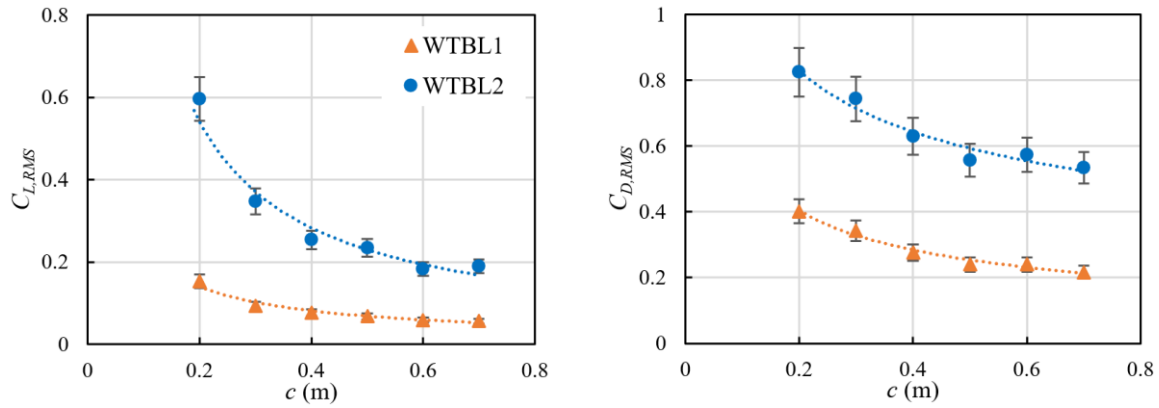

(a) (b)

Figure 8: The effect of the characteristic length dimension of the flat plate on the unsteady wind loads in two simulated wind tunnel boundary layers, (a) The fluctuating lift coefficient, $C_{L,RMS}$, on a horizontal flat plate, (b) The fluctuating drag coefficient, $C_{D,RMS}$, on a vertical flat plate (WTBL1: I_u=11%, L_u^x=0.57 m, I_w=8.9%, L_w^x=0.236 m; WTBL2, I_u=26%, L_u^x=0.81 m, I_w=21.1%, L_w^x=0.333 m).

In order to understand the correlation between the incoming turbulence and the forces on the flat plates of different characteristic lengths, the aerodynamic admittance function of the lift and drag force is evaluated. The aerodynamic admittance represents a measure of the effectiveness of a body in extracting energy from the oncoming turbulence at different frequencies (Larose and Livesey, 1997), and correlates the power spectrum of velocity with the power spectrum of the transverse force on the body. While in a quasi-steady situation the contribution of velocity fluctuations of all wavelengths is assumed equal in generation of aerodynamic forces, in reality, different scales of turbulence are not equally effective in producing aerodynamic forces (Sankaran and Jancauskas, 1992). The frequency-dependency of the aerodynamic forces is expressed by the aerodynamic admittance. The aerodynamic admittance of the transverse force on a flat plate is found from the following equation (Drabble *et al.*, 1990):

$$|A_i(f)|^2 = \frac{U^2 S_{C_i}(f)}{C_i^2 S_{jj}(f)}, \quad i = L, D, \ \ j = u, w \tag{3}$$

where $S_{jj}(f)$ and $S_{C_i}(f)$ represent the power spectra of the transverse velocity component, and transverse fluctuating force coefficient on the flat plate. For the vertical flat plate, the

aerodynamic admittance correlates the power spectrum of the drag force coefficient with the power spectrum of the longitudinal velocity, i.e. $|A_D(f)|^2 = \frac{U^2 S_{C_D}(f)}{C_D^2 S_{uu}(f)}$ (Bearman, 1971). For the horizontal flat plate, Larose and Livesey (1997) gives the aerodynamic admittance of the lift force as $|A_L(f)|^2 = \frac{U^2 S_{C_L}(f)}{4C_L^2 S_{uu}(f) + C'^2_L S_{ww}(f)}$, where C_L and $C'_L = \partial C_L/\partial\alpha$ represent the lift coefficient at zero angle of attack and the rate of change of the lift coefficient with the angle of attack (the slope of the lift curve for α=0), respectively. The experimental results, however, show that C_L is much smaller than C'_L (Larose *et al.*, 1998; Rasmussen *et al.*, 2010). Similarly, by measuring the lift force on the flat plates at low angles of attack near zero (between ±5°), in this study, C_L and C'_L were found to be -0.11 and 2.9, respectively. As given in the denominator of the equation given by Larose and Livesey (1997), the longitudinal velocity spectrum is weighed by $C_{L,0}^2$ and the vertical velocity spectrum is weighed by C'^2_L. Since $C_{L,0}^2$ is two orders of magnitude smaller than C'^2_L, the first term in the denominator (i.e., $4C_{L,0}^2\, S_{uu}(f)$) is much smaller than the second term (i.e., $C'^2_L\, S_{ww}(f)$). Hence, the equation given by Larose and Livesey (1997) can be simplified to the form given in Equation (3), as $|A_L(f)|^2 = \frac{U^2 S_{C_L}(f)}{C'^2_L S_{ww}(f)}$. This simplification of the aerodynamic admittance of the lift force is in agreement with the findings in the literature (Rasmussen *et al.*, 2010; Jafari *et al.*, 2018; Pfahl, 2018) reporting that the fluctuating lift force on the horizontal flat plate is mainly induced by the vertical velocity component of the turbulent eddies. In the present study, the aerodynamic admittance of the lift force has been calculated from the equation given by Larose and Livesey (1997) considering both longitudinal and vertical velocity spectra.

The aerodynamic admittance of the unsteady transverse forces on the flat plates are presented in Figure 9 as a function of reduced frequency, fc/U, where c is the characteristic length of the plate. The aerodynamic admittance of the lift force on the horizontal flat plates within the two WTBLs are shown in Figure 9(a–b), and the aerodynamic admittance of the drag force on the vertical flat plates are presented in Figure 9(c–d). According to Figure 9, as the reduced frequency increases, the aerodynamic admittance tends to zero which indicates that the higher frequencies of the turbulence spectrum contribute little to the overall force. The fluctuating transverse force is mainly induced by the lower reduced frequencies for which the admittance function is largest. For instance, according to Figure 9(a), the aerodynamic admittance of the lift force varies between 0.5 and 2 for c=0.2 m, between 0.6 and 1.5 for c=0.5 m, and between 0.4 and 1 for c=0.7 m, for reduced frequencies below 0.5. The aerodynamic admittance

decreases with further increase of the reduced frequency. A similar trend is found for the aerodynamic admittance of the forces for the plates in WTBL2. Reduction of the admittance function from its peak shows smaller correlation between the velocity of the turbulent eddies and the generated transverse force.

The observed trend is in agreement with that reported in the literature (Bearman, 1971; Drabble *et al.*, 1990; Larose *et al.*, 1998; Rasmussen *et al.*, 2010). For comparison of the calculated aerodynamic admittance in this study with the literature, the theoretical approximation of the aerodynamic admittance of the lift force for a flat plate in a fully correlated sinusoidal gust by Liepmann, calculated according to Fung (2002), is shown in Figure 9(a–b). The calculated aerodynamic admittance functions of the flat plates in the wind tunnel boundary layers show a similar trend to Liepmann's approximation, although larger in magnitude. Rasmussen *et al.* (2010) also reports that the admittance measured in wind tunnel experiments with spire-roughness-generated boundary layers is generally larger than Liepmann's approximation. Furthermore, the experimental results for a bridge deck model in a turbulent boundary layer with I_w=8% from Larose and Mann (1998) are shown in Figure 9(a), which demonstrate a similar decreasing trend with increasing fc/U, as observed for the flat plates in this study. Moreover, The aerodynamic admittance reported by Bearman (1971) for the drag force on a vertical flat plate in a grid-generated turbulence with I_u=8% and L_u^x/c=1.5 is also given in Figure 9(c). The aerodynamic admittance of the drag force found in this study follows the same trend as that given by Bearman (1971).

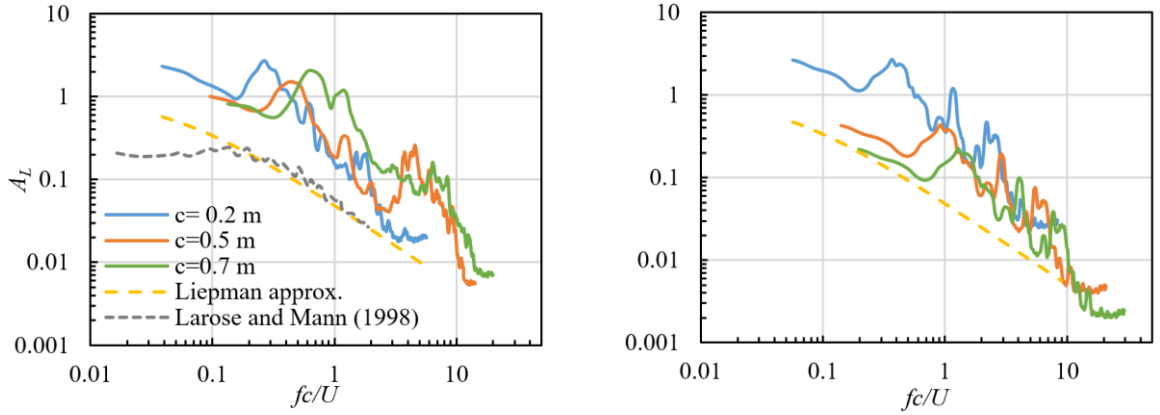

(a) (b)

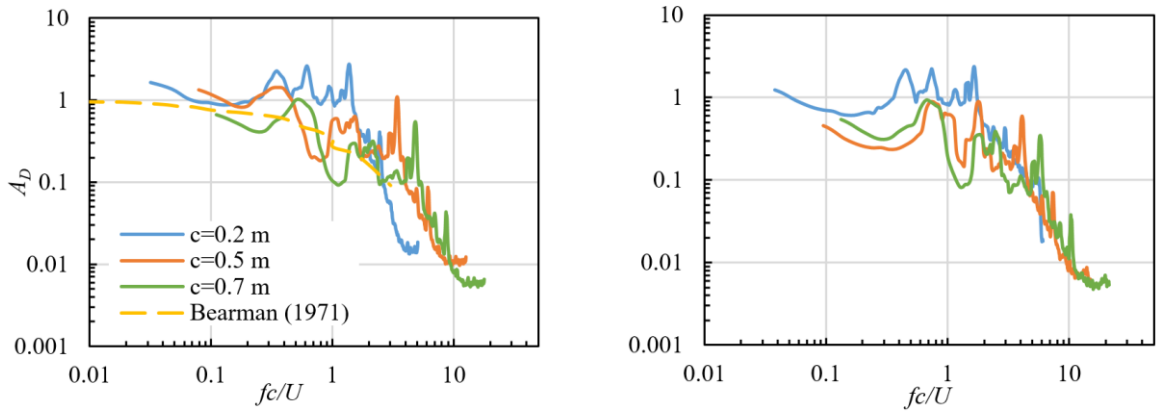

Figure 9: The aerodynamic admittance of the transverse force as a function of reduced frequency, fc/U, for different chord length dimensions of the flat plate, (a–b) lift force on the horizontal flat plate in WTBL1 and WTBL2, respectively, (c–d) the drag force on the vertical flat plate in WTBL1 and WTBL2, respectively (WTBL1: I_u=11%, L_u^x=0.57 m, I_w=8.9%, L_w^x=0.236 m; WTBL2, I_u=26%, L_u^x=0.81 m, I_w=21.1%, L_w^x=0.333 m).

According to Figure 9, the aerodynamic admittance decreases sharply from its peak as the reduced frequency increases to values of above approximately 1. This trend holds true for all the flat plates in both WTBLs despite the difference in the magnitude of the aerodynamic admittance for flat plates of different characteristic length dimensions. Since the peak of the aerodynamic admittance (which has a magnitude near 1) shows the strongest correlation between the transverse force and the turbulence spectra, it can be concluded that turbulence eddies with reduced frequencies lower than 1 are more effective in generating the transverse force. The reason is that turbulence fluctuations with reduced frequencies above 1 are less spatially correlated. Hence, the critical reduced frequencies, which are the major contributors to the fluctuating force are approximately below 1 for all the investigated cases. This is in agreement with the findings by Drabble *et al.* (1990) who compared the aerodynamic admittance of the drag force on a vertical flat plate in a turbulent flow with that in a fully coherent fluctuating flow. It was found that in the turbulent flow, the aerodynamic admittance decreased rapidly for reduced frequencies above approximately 0.5, while the admittance increased with increasing frequency in the fully coherent fluctuating flow (Drabble *et al.*, 1990).

It must be noted that the minor peaks observed at higher frequencies are due to the body-induced turbulence as also noted by Rasmussen *et al.* (2010). Furthermore, the lower band of the calculated values shown in Figure 9 is limited to half of the sampling frequency of the force and velocity measurements, which is identical for all the cases. However, the different low bands for fc/U in Figure 9 are due to normalising this frequency with c and U, which differ for the different flat plate and the WTBLs, respectively.

The difference in the magnitude of the aerodynamic admittance of flat plates with different characteristic length dimensions, seen in Figure 9, shows the effect of the ratio of the turbulence length scales to the plate's characteristic length. As more clearly demonstrated in Figure 9(b), the magnitude of the lift force aerodynamic admittance, especially at low frequencies, is largest for c=0.2 m, for which the ratio of length scale of turbulence over c is the largest. Similarly, the magnitude of the aerodynamic admittance of the drag force is largest for c=0.2 m (see Figure 9(d)). This is due to the stronger correlation of the turbulent fluctuations over the plate's characteristic length. Larose *et al.* (1998) also found that the aerodynamic admittance of lift force on bridge decks was larger for decks with larger ratio of vertical integral length scale over the deck's characteristic length (L_w^x/c). Hence, as shown in Figures (8–9), the fluctuating transverse force and its aerodynamic admittance are larger on the flat plate with a smaller characteristic length dimension. As evaluation of the aerodynamic admittance function shows that reduced frequencies below 1 are responsible for the generation the fluctuating force, the larger transverse force on the flat plate with a smaller characteristic length dimension is related to the larger magnitude of the turbulence energy over this spectral range, compared to the larger plates. This is demonstrated in Figure 10 which presents the velocity power spectra normalised by the mean velocity as a function of reduced frequency, fc/U, for chords of c=0.2 m, c=0.5 m and c=0.7 m. As shown in the Figure 10, there is a shift to lower reduced frequencies for flat plates with smaller characteristic length dimension. Larger longitudinal and vertical turbulence energy over the critical reduced frequency range for c=0.2 m lead to increasing the fluctuating drag and lift force, respectively. Hence, an accurate estimation of the fluctuating force on a horizontal flat-plate-like structure in a wind tunnel experiment can be achieved if the distribution of vertical power spectrum as a function of reduced frequency is a close match to that of the full scale over the critical reduced frequency range below 1. Similarly, for an accurate estimation of the fluctuating drag force on a vertical flat plate, an appropriate characteristic length for the model should be chosen such that the distribution of longitudinal turbulence spectrum over the critical reduced frequency range is a close match to that at the full scale.

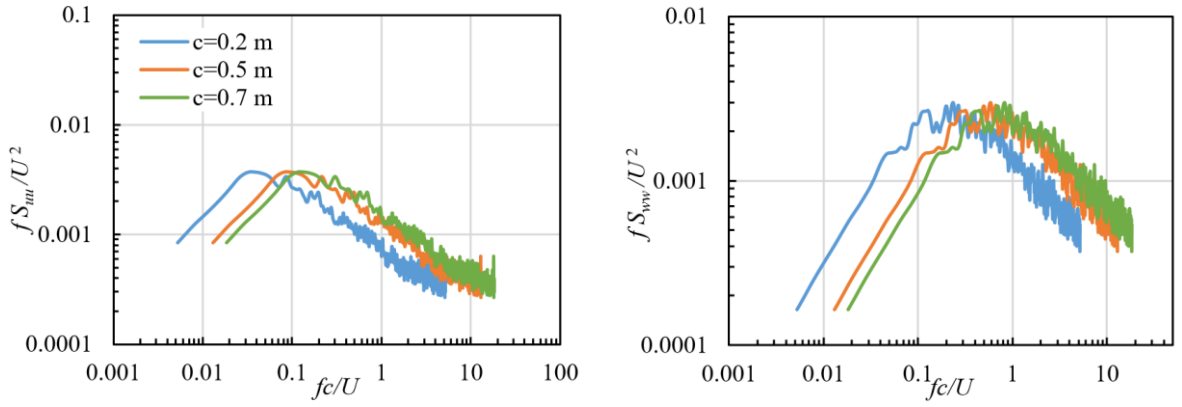

(a) (b)

Figure 10: The normalised power spectral density of turbulence energy as a function of reduced frequency, fc/U, for different characteristic length dimensions of the flat plate in WTBL1 at z=0.3 m (a) normalised longitudinal power spectrum, fS_{uu}/U^2, (b) normalised vertical power spectrum, fS_{ww}/U^2.

5 Discussion

The spectral analysis presented in Section 4 shows the existence of a range of reduced frequencies, which are critical to the generation of the unsteady wind loads. This indicates that the critical turbulence frequency range, and the corresponding critical length scales of turbulence which influence the fluctuating wind loads, are dependent on the characteristic length of the model. This relationship is expressed by normalising the turbulence frequency with the characteristic length of the structure, in terms of reduced frequency. The results from the wind tunnel experiments on horizontal and vertical flat plates of various dimensions, given in Section 4, show that the wind loads are mainly generated by the turbulence length scales over the range of reduced frequencies below 1, i.e., $fc/U \leq 1$, which represents turbulent eddies which are of approximately the same length scale of the structure. The reason for this is that the turbulent eddies which are much smaller than the flat plate's characteristic length do not correlate over the structure's length and therefore do not produce large loads. The eddies which are of approximately the same order as the plate produce large unsteady loads on it.

On the other hand, the studies in the literature suggest that the eddies which are much larger than the structure, $fc/U \ll 1$, do not produce significant loads on it either. According to the studies in the literature (Lee, 1975; Holdø *et al.*, 1982; Bearman and Morel, 1983), when the turbulence length scale is much larger than the characteristic length of the structure, free-stream turbulence acts like a correlated unsteady mean flow and the flow behaviour around the body is quasi-static. The turbulence scales which interact with the local flow field, not the eddies with very larger scales, produce the unsteady wind loads (Richards *et al.*, 2007). However, the effect of the very large scales could not be investigated in the performed analysis as the results

from the wind tunnel experiments are limited at the low frequency range due to the sampling frequencies and the restriction in generation of the low-end of the spectrum in the wind tunnel. Consequently, the smallest reduced frequency for which the aerodynamic admittance was calculated was approximately 0.03 (as shown in Figure 9). Therefore, it can be concluded from the experimental results of this study and the studies in the literature that turbulent length scales corresponding to a range of reduced frequencies between 0.01 and 1, are most effective in generation of the unsteady wind loads. Hence, it is proposed that this range of reduced frequencies of the turbulence spectrum should be correctly modelled in wind tunnel experiments in order to minimise the scaling effects. The suitable geometric scaling ratio of the structure should then be determined based on the scaling ratio for which the turbulence spectrum as a function of reduced frequency is the closest match to that at full-scale.

The critical reduced frequency range determined in this study is in agreement with the experimental results in the literature. For instance, Richards *et al.* (2007) compared the pressure distribution on a cubic model in a wind tunnel experiment with the data collected on the full-scale Silsoe cube, and reported that when the mid- to high-frequency ranges of the turbulence spectra in the wind tunnel matched the full-scale spectra, the obtained pressure coefficients from the wind tunnel experiment were a close match to the full-scale data. The frequency range, referred to as the mid- to high-frequency range by Richards *et al.* (2007), corresponds to $fc/U > 0.05$ for the longitudinal spectrum (Figure 11(a)). This range contains the critical frequency range obtained from the results of the present study, $0.01 < fc/U < 1$, (shaded in Figure 11(a)) which shows that by matching the spectra in the wind tunnel to the full-scale over this reduced frequency range, the wind tunnel experimental results provided a good match to the full-scale pressure measurements. This is in agreement with the concluded result in the present study that the critical reduced frequency range is the major contributor to the wind loads. Furthermore, comparison of the pressure distribution on a cubic model, measured from six wind tunnel studies with similar simulated boundary layers (Hölscher and Niemann, 1998), with the full-scale pressure measurements from Silsoe cube showed that the results were the closest to the full-scale pressure coefficients for two wind tunnel experiments, for which the turbulence spectrum was a closer match to the full-scale spectrum for reduced frequencies above approximately 0.1 (Figure 11(b) based on the spectra given by (Richards *et al.*, 2007)). Moreover, a similar partial simulation approach was recommended by Irwin (2008) for wind tunnel modelling of bridge decks is in agreement with the results of this study. Irwin (2008) suggested matching only a higher frequency range of the turbulence spectrum with the full-scale. The recommended high-frequency range for the bridge decks corresponds to reduced

frequencies between approximately 0.1 and 1 which is in agreement with matching the critical reduced frequency range found in the present study. As discussed above, the critical turbulence length scales and frequencies are a function of the characteristic dimension of the structure. This explains the reason why the recommended critical frequencies for the bridge decks by Irwin (2008) contain higher frequencies as follows. Due to the larger characteristic length of the bridge decks, the critical reduced frequency range, $0.01< fc/U <1$, contains mainly the high-end frequency of the turbulence spectrum. For small-scale structures, such as solar panels, due to the smaller characteristic length, this range of reduced frequencies will shift to slightly larger length scales of turbulence containing mid- to high-frequencies.

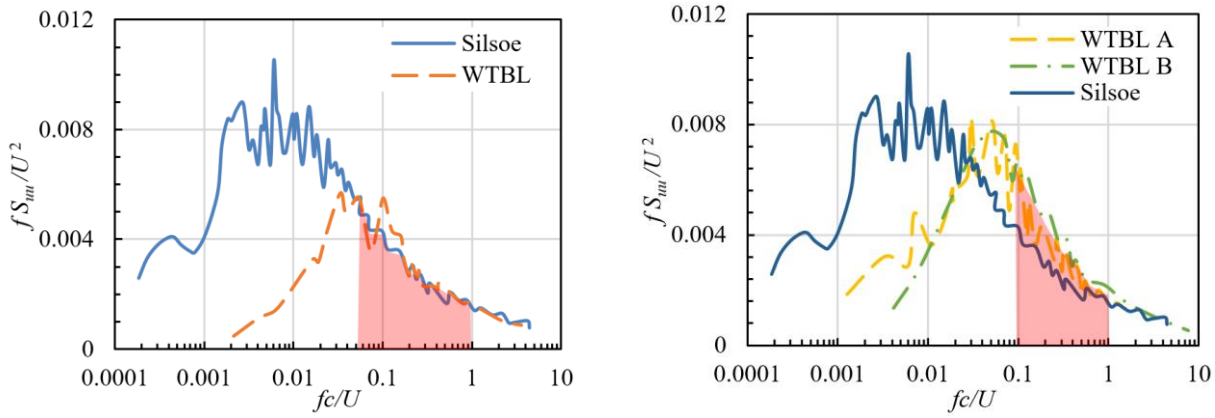

(a) (b)

Figure 11: The turbulence power spectra as a function of reduced frequency compared with the Silsoe site, for (a) The Auckland wind tunnel (Richards *et al.*, 2007), (b) Two different wind tunnel experiments (Hölscher and Niemann, 1998) reproduced from (Richards *et al.*, 2007). The red shaded area represents the critical reduced frequency range.

In order to demonstrate an example of the application of the results, the case of the flat plate mentioned in Section 3.1 is considered. Figure 12 shows the turbulence spectra of WTBL1 as a function of reduced frequency for different scaling ratios of the model compared to the full-scale spectra. The full-scale spectra were estimated from the modified Von Karman model by ESDU85020 (2010) and for an open-country terrain with a surface roughness of approximately 0.02 m and a mean velocity of 20 m/s. According to Figure 12(a), for model scaling ratios of 1:24 and 1:17 (a characteristic length dimension of 0.5 m and 0.7 m for the plate, respectively), a close match to the longitudinal spectrum for fc/U of between 0.1 and 1 is achieved, while a smaller model scaling ratio of 1:60 leads to a noticeable mismatch in the turbulence spectrum. Therefore, geometric scaling ratios of 1:24 and 1:17 can be used for measurement of the unsteady drag on the vertical flat plate. For the horizontal configuration of the flat plate, however, the vertical turbulence spectrum is more important. According to Figure 12(b), the

closest match to the vertical turbulence spectrum can be achieved for the scaling ratio of 1:60. Using larger geometric scaling for the model leads to underestimation of the unsteady lift force on the stowed flat plate. Hence, for measurement of the unsteady drag force on the vertical flat plate, larger model scales can be used, while measurement of the unsteady lift force on the horizontal flat plate requires smaller model scales which is mainly due to the restricted generation of the vertical turbulence structures in the wind tunnel. The model scale should therefore be chosen according to the full-scale conditions and the WTBL turbulence characteristics for each case.

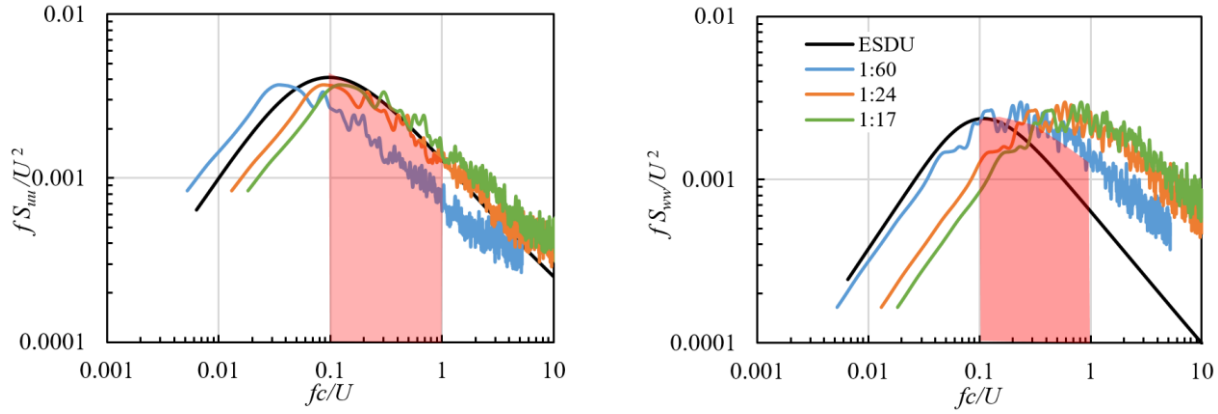

Figure 12: The effect of model scale on the mismatch of turbulence spectra, (a) The normalised power spectral density of longitudinal turbulence energy, fS_{uu}/U^2, (b) The normalised power spectral density of vertical turbulence energy, fS_{ww}/U^2, as a function of reduced frequency, fc/U. The red shaded area represents the critical reduced frequency range.

The effect of the turbulence spectrum on the unsteady wind loads and the dependency of the drag and lift coefficients on the critical reduced frequency range of the longitudinal and vertical turbulence spectra show the importance of matching the turbulence parameters in the wind tunnel experiments to those at full-scale. The obtained results suggest the possibility of achieving a unified wind load coefficient valid for all geometric scales by normalising the wind force with the turbulence characteristics of the flow. A similar approach was used by Richards *et al.* (2007) to normalise the pressure coefficient by the peak dynamic pressure instead of the mean dynamic pressure, and in this way, the effect of turbulence intensity was taken into account. However, further wind load measurements on full-scale structures are required to assess the applicability of normalisation of the forces with turbulence intensity and length scales.

6 Conclusion

The effect of mismatch of turbulence spectra on the unsteady wind loads in wind tunnel modelling of small-scale structures was investigated in this study. Wind loads on horizontal and vertical flat plates were measured in two simulated atmospheric boundary layers in a large-scale wind tunnel. The results showed that wind loading is frequency-dependant. It was found through spectral analysis that the turbulent eddies within a range of reduced frequencies between approximately 0.01 and 1 contributed the most to the unsteady wind loads on the flat plates. Based on the experimental results, it was proposed that this range of reduced frequencies of the turbulence spectrum should be correctly modelled in a wind tunnel experiment in order to minimise the scaling effects. The suitable geometric scaling ratio of the structure should then be determined based on the scaling ratio for which the turbulence spectrum as a function of reduced frequency is the closest match to that at full-scale.

The results were applied for determination of a suitable scaling ratio for wind tunnel modelling of a flat-plate like structure such as a solar tracker or heliostat as a case study. It was found that larger model dimensions could be used for measurement of the unsteady drag force on the vertical flat plate, while measurement of the unsteady lift force on the horizontal plate required models scaled down to smaller dimensions.

Acknowledgements

Financial support for the project has been provided by the Australian Government Research Training Program, the University of Adelaide Scholarship and the Australian Solar Thermal Research Initiative (ASTRI). The authors would like to acknowledge the School of Mechanical Engineering and the workshop at the University of Adelaide.

References

Aly, A. M., and Bitsuamlak, G. 2013. Aerodynamics of ground-mounted solar panels: Test model scale effects, *Journal of Wind Engineering and Industrial Aerodynamics*, 123: 250-60.

Bearman, P. W. 1971. An investigation of the forces on flat plates normal to a turbulent flow, *Journal of Fluid Mechanics*, 46: 177-98.

Bearman, P. W., and Morel, T. 1983. Effect of free stream turbulence on the flow around bluff bodies, *Progress in Aerospace Sciences*, 20: 97-123.

Bronkhorst, A., Franke, J., Geurts, C., van Bentum, C., and Grépinet, F. 2010. Wind tunnel and CFD modelling of wind pressures on solar energy systems on flat roofs. In *The fifth International Symposium on Computational Wind Engineering*.

Cook, N. J. 1978. Determination of the model scale factor in wind-tunnel simulations of the adiabatic atmospheric boundary layer, *Journal of Wind Engineering and Industrial Aerodynamics*, 2: 311-21.

Davenport, A. G. 1960. Rationale for determining design wind velocities, *ASCE Journal of the Structural Division*, 86: 39-68.

De Paepe, W., Pindado, S., Bram, S., and Contino, F. 2016. Simplified elements for wind-tunnel measurements with type-III-terrain atmospheric boundary layer, *Measurement*, 91: 590-600.

Drabble, M. J., Grant, I., Armstrong, B. J., and Barnes, F. H. 1990. The aerodynamic admittance of a square plate in a flow with a fully coherent fluctuation, *Physics of Fluids A: Fluid Dynamics*, 2: 1005-13.

Drobinski, P., Carlotti, P., Newsom, R. K., Banta, R. M., Foster, R. C., and Redelsperger, J.-L. 2004. The structure of the near-neutral atmospheric surface layer, *Journal of the Atmospheric Sciences*, 61: 699-714.

Dyrbye, C., and Hansen, S. O. 1996. *Wind Loads on Structures*, John Wiley & Sons.

Emes, M. J., Arjomandi, M., Ghanadi, F., and Kelso, R. M. 2017. Effect of turbulence characteristics in the atmospheric surface layer on the peak wind loads on heliostats in stow position, *Solar Energy*, 157: 284-97.

ESDU85020. 2010. Characteristics of atmospheric turbulence near the ground - Part II: single point data for strong winds (neutral atmosphere), *Engineering Sciences Data Unit*.

Fritz, W. P., Bienkiewicz, B., Cui, B., Flamand, O., Ho, T. C., Kikitsu, H., Letchford, C. W., and Simiu, E. 2008. International comparison of wind tunnel estimates of wind effects on low-rise buildings: Test-related uncertainties, *Journal of Structural Engineering*, 134: 1887-90.

Fung, Y. C. 2002. *An Introduction to the Theory of Aeroelasticity*, Dover Publications.

Högström, U., Hunt, J. C. R., and Smedman, A.-S. 2002. Theory and measurements for turbulence spectra and variances in the atmospheric neutral surface layer, *Boundary-Layer Meteorology*, 103: 101-24.

Holdø, A. E., Houghton, E. L., and Bhinder, F. S. 1982. Some effects due to variations in turbulence integral length scales on the pressure distribution on wind-tunnel models of low-rise buildings, *Journal of Wind Engineering and Industrial Aerodynamics*, 10: 103-15.

Holmes, J. D. 2007. *Wind Loading of Structures*, Taylor & Francis.

Hölscher, N., and Niemann, H.-J. 1998. Towards quality assurance for wind tunnel tests: A comparative testing program of the Windtechnologische Gesellschaft, *Journal of Wind Engineering and Industrial Aerodynamics*, 74-76: 599-608.

Hunt, A. 1982. Wind-tunnel measurements of surface pressures on cubic building models at several scales, *Journal of Wind Engineering and Industrial Aerodynamics*, 10: 137-63.

Irwin, H. P. A. H. 1981. The design of spires for wind simulation, *Journal of Wind Engineering and Industrial Aerodynamics*, 7: 361-66.

Irwin, P. A. 2008. Bluff body aerodynamics in wind engineering, *Journal of Wind Engineering and Industrial Aerodynamics*, 96: 701-12.

Jafari, A., Ghanadi, F., Arjomandi, M., Emes, M. J., and Cazzolato, B. S. 2018. The effect of turbulence intensity and length scale on the peak lift force on flat plates in longitudinal flows, *Journal of Wind Engineering and Industrial Aerodynamics (Under review)*.

Jafari, A., Ghanadi, F., Arjomandi, M., Emes, M. J., and Cazzolato, B. S. 2019. Correlating turbulence intensity and length scale with the unsteady lift force on flat plates in an atmospheric boundary layer flow, *Journal of Wind Engineering and Industrial Aerodynamics*, 189: 218-30.

Jafari, A., Ghanadi, F., Emes, M. J., Arjomandi, M., and Cazzolato, B. S. 2018. Effect of free-stream turbulence on the drag force on a flat plate. In *21st Australasian Fluid Mechanics Conference*. Adelaide, Australia.

Kozmar, H. 2011. Truncated vortex generators for part-depth wind-tunnel simulations of the atmospheric boundary layer flow, *Journal of Wind Engineering and Industrial Aerodynamics*, 99: 130-36.

Kozmar, H. 2012. Physical modeling of complex airflows developing above rural terrains, *Environmental Fluid Mechanics*, 12: 209-25.

Larose, G. L., and Livesey, F. M. 1997. Performance of streamlined bridge decks in relation to the aerodynamics of a flat plate, *Journal of Wind Engineering and Industrial Aerodynamics*, 69-71: 851-60.

Larose, G. L., and Mann, J. 1998. Gust loading on streamlined bridge decks *Journal of Fluids and Structures*, 12: 511-36.

Larose, G. L., Tanaka, H., Gimsing, N. J., and Dyrbye, C. 1998. Direct measurements of buffeting wind forces on bridge decks, *Journal of Wind Engineering and Industrial Aerodynamics*, 74-76: 809-18.

Lee, B. E. 1975. Some effects of turbulence scale on the mean forces on a bluff body, *Journal of Wind Engineering and Industrial Aerodynamics*, 1: 361-70.

Peterka, J. A., Tan, Z., Cermak, J. E., and Bienkiewicz, B. 1989. Mean and peak wind loads on heliostats, *Journal of solar energy engineering*, 111: 158-64.

Pfahl, A. 2018. Wind loads on heliostats and photovoltaic trackers, *Eindhoven: Technische Universiteit Eindhoven*.

Pfahl, A., Buselmeier, M., and Zaschke, M. 2011. Wind loads on heliostats and photovoltaic trackers of various aspect ratios, *Solar Energy*, 85: 2185-201.

Radu, A., Axinte, E., and Theohari, C. 1986. Steady wind pressures on solar collectors on flat-roofed buildings, *Journal of Wind Engineering and Industrial Aerodynamics*, 23: 249-58.

Rasmussen, J. T., Hejlesen, M. M., Larsen, A., and Walther, J. H. 2010. Discrete vortex method simulations of the aerodynamic admittance in bridge aerodynamics, *Journal of Wind Engineering and Industrial Aerodynamics*, 98: 754-66.

Richards, P. J., Hoxey, R. P., Connell, B. D., and Lander, D. P. 2007. Wind-tunnel modelling of the Silsoe Cube, *Journal of Wind Engineering and Industrial Aerodynamics*, 95: 1384-99.

Roy, R. J., and Holmes, J. D. 1988. The effects of scale distortion on total wind loads on a low rise building model, *Journal of Wind Engineering and Industrial Aerodynamics*, 29: 273-82.

Ruscheweyh, H., and Windhövel, R. 2011. Wind loads at solar and photovoltaic modules for large plants. In *13th International Conference on Wind Engineering (ICWE)*. Amsterdam, Netherlands.

Saha, p. K., Yoshida, A., and Tamura, Y. 2011. Study on wind loading on solar panel on a flat-roof building: Effects of locations and inclination angles. In *13th International Conference on Wind Engineering (ICWE)*. Amsterdam, Netherlands.

Sankaran, R., and Jancauskas, E. D. 1992. Direct measurement of the aerodynamic admittance of two-dimensional rectangular cylinders in smooth and turbulent flows, *Journal of Wind Engineering and Industrial Aerodynamics*, 41: 601-11.

Stathopoulos, T., and Surry, D. 1983. Scale effects in wind tunnel testing of low buildings, *Journal of Wind Engineering and Industrial Aerodynamics*, 13: 313-26.

Stathopoulos, T., Zisis, I., and Xypnitou, E. 2012. Wind loads on solar collectors: A review. in, *Proceedings of Structures Congress 2012*.

Tieleman, H. W. 2003. Wind tunnel simulation of wind loading on low-rise structures: A review, *Journal of Wind Engineering and Industrial Aerodynamics*, 91: 1627-49.

Wooding, R. A., Bradley, E. F., and Marshall, J. K. 1973. Drag due to regular arrays of roughness elements of varying geometry, *Boundary-Layer Meteorology*, 5: 285-308.